



A Measurement of Z Forward-Backward Asymmetry with 364 pb^{-1} of CDF Run II Data

The CDF Collaboration
URL <http://www-cdf.fnal.gov>
(Dated: July 23, 2006)

We present a measurement of the Z boson forward-backward charge asymmetry of the process $p\bar{p} \rightarrow \gamma^*/Z + X \rightarrow e^+e^- + X$, where the mass of the intermediate γ^*/Z has invariant mass above 30 GeV. The measurement uses 364 pb^{-1} of CDF Run II data. The method of matrix inversion is used to correct for the distortion in the measurement caused by the detector resolution and photon radiation in the final state. The measurement is consistent with the Standard Model prediction with χ^2/ndof 10.9/12.

Preliminary Results for Summer 2006 Conferences

I. INTRODUCTION

The process $p\bar{p} \rightarrow l^+l^-X$ is mediated by the electroweak neutral current, which is an interference between the photon γ and Z boson exchange. The vertex factor of the interaction $Z \rightarrow l^+l^-$ is expressed as following.

$$-i\frac{g}{\cos\theta_W}\gamma^\mu(c_V^l - c_A^l\gamma^5), \quad (1)$$

where c_V^l and c_A^l are the vector and axial-vector couplings of the lepton to the Z boson. The presence of both vector and axial-vector components gives rise to an asymmetry in the polar angle of the outgoing lepton θ in the rest frame of the lepton pair.

The differential cross section of $q\bar{q} \rightarrow l^+l^-X$ can be written in terms of the electron scattering angle θ as following.

$$\frac{d\sigma}{d\cos\theta} = \frac{4\pi\alpha^2}{3s} \left[\frac{3}{8}A(1 + \cos^2\theta) + B\cos\theta \right], \quad (2)$$

where

$$\begin{aligned} A &= Q_l^2 Q_q^2 + 2Q_l Q_q g_V^q g_V^l \text{Re}(\chi(s)) + g_V^{l^2} (g_V^{q^2} + g_A^{q^2}) |\chi(s)|^2 + g_A^{l^2} (g_V^{q^2} + g_A^{q^2}) |\chi(s)|^2, \\ B &= \frac{3}{2} g_A^q g_A^l (Q_l Q_q \text{Re}(\chi(s)) + 2g_V^q g_V^l |\chi(s)|^2), \\ \chi(s) &= \frac{1}{\cos^2\theta_W \sin^2\theta_W} \frac{s}{s - M_Z^2 + i\Gamma_Z M_Z}, \end{aligned}$$

$Q_{l,q}$ is the electric charge of lepton or quark and s is the center-of-momentum system energy of the incoming $q\bar{q}$ system. The angular asymmetry may be measured by the forward-backward asymmetry A_{FB} , which is defined as following.

$$A_{FB} = \frac{\int_0^{+1} \frac{d\sigma}{d\cos\theta} d\cos\theta + \int_{-1}^0 \frac{d\sigma}{d\cos\theta} d\cos\theta}{\int_{-1}^{+1} \frac{d\sigma}{d\cos\theta} d\cos\theta} = \frac{B}{A}. \quad (3)$$

Therefore a measurement of A_{FB} is a direct probe of the relative strength of the vector and axial-vector structure of the electroweak interaction. A_{FB} is connected to the measurables as following.

$$A_{FB} = \frac{\sigma_F - \sigma_B}{\sigma_F + \sigma_B}. \quad (4)$$

The scattering angle of the outgoing lepton can be unambiguously measured in the absence of the transverse momentum of the incoming quarks. One can take the direction of the incoming proton beam as the polar axis and the angle can be measured from the four momenta of the outgoing leptons. However in the presence of the transverse momentum of the quarks, we adopt the Collins-Soper formalism to minimize the effect of the transverse momentum of the incoming quarks.

With the formalism, the polar axis is defined as the bisector of the proton beam momentum and the negative of the anti-proton beam momentum when they are boosted into the center-of-mass frame of the electron-positron pair. The scattering angle of the outgoing electron θ^* is defined as the angle between the electron and the polar axis. Then $\cos\theta^*$ is given by

$$\cos\theta^* = \frac{2}{Q\sqrt{Q^2 + Q_T^2}} (P_1^+ P_2^- - P_1^- P_2^+), \quad (5)$$

where Q (Q_T) is the four momentum (transverse momentum) of the electron-positron pair. P_i^\pm is defined to be $\frac{1}{\sqrt{2}}(P_i^0 \pm P_i^3)$, where P^0 and P^3 represent energy and the longitudinal components of the momentum, and $i = 1, 2$ represent electron and positron, respectively. Forward and backward events are defined by the sign of $\cos\theta^*$.

We measure A_{FB} in twelve dielectron invariant mass (M_{ee}) ranges. The measurement is complicated by detector resolution and QED radiation which cause the true and measured M_{ee} and $\cos\theta^*$ differ. The correction needs to be made in order to unfold the detector effect. The method of matrix inversion is one of the unfolding methods, which is chosen for this analysis for its simplicity and lack of bias. Suppose the true numbers of events in the invariant mass bin j is μ_j . We will refer to the vector $\boldsymbol{\mu} = (\mu_1, \dots, \mu_N)$ as the true histogram. Note that these are the numbers of expectation values, rather than the actual numbers of events in the various bins. The vector $\boldsymbol{\mu}$ is what we want to

measure by unfolding. The observed values is $\mathbf{n} = (n_1, \dots, n_N)$. It is possible to regard the variables n_i as independent Poisson variables with expectation values $\nu_i = E[n_i]$. That is, for this model the probability to observe n_i events in bin i is given by

$$P(n_i; \nu_i) = \frac{\nu_i^{n_i} e^{-\nu_i}}{n_i!}. \quad (6)$$

The expected number of events to be observed in bin i can be written as

$$\nu_i = \sum_{j=1}^N R_{ij} \mu_j, \quad (7)$$

where

$$\begin{aligned} R_{ij} &= \frac{P(\text{observed in bin } i \text{ and true value in bin } j)}{P(\text{true value in bin } j)} \\ &= P(\text{observed in bin } i \mid \text{true value in bin } j). \end{aligned} \quad (8)$$

The response matrix element R_{ij} is thus the conditional probability that an event will be found in bin i given that the true value was in bin j . The effect of off-diagonal elements in R is to smear out any fine structure. Summing over the first index gives

$$\sum_{i=1}^N R_{ij} \equiv \varepsilon_j, \quad (9)$$

i.e., one obtains the average value of the efficiency over bin j . If the expectation value for the background process in bin i is known, the vectors $\boldsymbol{\mu}$, $\boldsymbol{\nu}$, $\boldsymbol{\beta}$ and the matrix R are related by $\boldsymbol{\nu} = R\boldsymbol{\mu} + \boldsymbol{\beta}$. The matrix relation can be inverted to give $\boldsymbol{\mu} = R^{-1}(\boldsymbol{\nu} - \boldsymbol{\beta})$. The estimators of $\boldsymbol{\nu}$ is given by the corresponding data value, $\hat{\boldsymbol{\nu}} = \mathbf{n}$. The estimators for the $\boldsymbol{\mu}$ are then

$$\hat{\boldsymbol{\mu}} = R^{-1}(\mathbf{n} - \boldsymbol{\beta}). \quad (10)$$

In order to unfold the distribution of A_{FB} , the number of forward events $\boldsymbol{\mu}^F$ and the backward events $\boldsymbol{\mu}^B$ are separately unfolded with two response matrices R^F and R^B , obtained from the forward and backward events from the Monte Carlo simulation. The smearing between forward and backward is correctly taken into account for the construction of R^F and R^B . The unfolded A_{FB} is therefore

$$A_{FB}^i = \frac{\mu_i^F - \mu_i^B}{\mu_i^F + \mu_i^B}, \quad (11)$$

where $\mu_i^{F,B} = R_{ij}^{(F,B)-1} \nu_j^{F,B}$. The statistical uncertainty for the unfolded number arises from the data ($\boldsymbol{\nu}$) and from the response matrix (R_{ij}^{-1}) as following.

$$(\sigma_{\mu_i})^2 = \sum_{j=1}^N \left(\frac{\partial \mu_i}{\partial \nu_j} \sigma_{\nu_j} \right)^2 + \sum_{j=1}^N \left(\frac{\partial \mu_i}{\partial R_{ij}^{-1}} \sigma_{R_{ij}^{-1}} \right)^2 = \sum_{j=1}^N (R_{ij}^{-1} \sigma_{\nu_j})^2 + \sum_{j=1}^N (\nu_j \sigma_{R_{ij}^{-1}})^2. \quad (12)$$

The uncertainties of the response matrix $\sigma_{R_{ij}^{-1}}$ is highly correlated due to the matrix inversion and are calculated as described in [1].

II. EVENT SELECTION

A. Monte Carlo Sample

Pythia version 6.216 with the parton distribution function CTEQ5L is used to generate ten million events with the mass of $\gamma^*/Z > 30$ GeV. The generator includes the interference between γ^* and the Z , as well as final state QED radiation. For the systematic effect of the material in the central tracking region ($|\eta| < 1.0$) The same generated events were run by a simulation with 1 % more material in the central tracking region at a radius of 15.0 cm. In addition we ran another simulation with 1/6 X_0 more material for the systematic study of the material in the plug region with $|\eta| > 1.0$.

Variable	Central	Plug
Fiduciality	1 or 2	$1.18 < \eta < 3.0$
track $ z_0 $	< 60 cm	N/A
E_T	> 25 GeV	> 25 GeV
p_T	> 15 GeV ($E_T < 100$ GeV) > 25 GeV ($E_T > 100$ GeV)	N/A
E_{had}/E_{em}	$< 0.055 + 0.00045 * E$	$< 0.05 + 0.026 * \log(E/100)$
E_T^{iso}	$< 3 + 0.02 * E_T$	$< 1.6 + 0.02 * E_T$
E/p	$< 2.5 + 0.015 * E_T$ ($E_T < 100$ GeV)	N/A
L_{shr}	< 0.2	N/A
$ \Delta x $	< 3 cm	N/A
$ \Delta z $	< 5 cm	N/A
$PEM\chi_{3x3}^2$	N/A	< 25

TABLE I: Selection cuts for the electron candidates.

B. Data

This analysis uses the data collected between Spring 2002 and Summer 2004, corresponding to 364 pb^{-1} of integrated luminosity. The analysis requires two electrons e^- and e^+ with at least one of them passing central electron triggers. The other electron is allowed to be found either in central or plug region. We find 9455 events with central-central (CC) combination and 13455 events with central-plug (CP) combination.

Central electrons are reconstructed from an energy deposit in the central electromagnetic calorimeter (CEM) where $|\eta_{det}| < 1.0$. The cuts listed in the Table I are applied to the reconstructed EM object. The energy is corrected for the intra-tower responses and tower-to-tower gain variations. The global energy scale is corrected so that the spectrum agrees with the prediction from M_Z as measured at LEP I. An electron is considered to be in the fiducial region of the detector if the matching track points within 60 cm in z of the center of the detector and extrapolates to the calorimeter away from the calorimeter wedge boundaries. The momentum (p_T) of the electron is determined by the highest p_T track associated with the EM cluster. The track four momentum is used for the calculation of the transverse component of the energy and the invariant mass of the electron pairs. The charge of the electron is determined from the curvature of the track. E_{had}/E_{em} is the ratio of the hadronic energy to the electromagnetic energy. E_T^{iso} is the total transverse energy within a radius of 0.4 in $\Delta R = \sqrt{\Delta\eta_{evt}^2 + \Delta\phi^2}$ of the cluster centroid, excluding the cluster energy itself. E/p is the ratio of the calorimeter energy to the momentum of the track, which deviates from 1.0 due to the detector material and detector resolution. L_{shr} is a measure of the difference in the lateral sharing of energy among the calorimeter towers, compared to the test beam electron data. $|\Delta x|$ and $|\Delta z|$ measure the distance in $r - \phi$ and z between the electron shower position and the extrapolated track position.

The plug electron is selected from the plug electromagnetic calorimeter (PEM) with $1.2 < |\eta_{det}| < 3.0$. The global energy scale is corrected in the same way as the central electron is corrected. The central outer tracker (COT) does not cover this region and we don't use the track information for the plug electron selection. The z position of the cluster reconstruction is provided by the primary vertex of the event. The selection criteria are listed in the Table I. $PEM\chi_{3x3}^2$ is calculated from the comparison of the energy distribution in 3×3 PEM towers around the seed tower to the distributions from the test electron beam.

III. BACKGROUND

A. Jet Background

One of major sources of the background to the process $p\bar{p} \rightarrow e^+e^-X$ is hadronic jets that are misidentified as electrons. Pions in jets can be misidentified as electrons, or jets can contain real electrons from semi-leptonic heavy-flavor decays. The amount of these backgrounds in the dielectron sample can be estimated from the fact that the electrons from the Z decay tend to be more isolated than the misidentified jets. In order to extract the number of jet background, the isolation distribution of the data is fitted to the sum of electron template and jet template.

Electron template is obtained by applying tight cuts to the events with the invariant mass within $10 \text{ GeV}/c^2$ around Z mass $91 \text{ GeV}/c^2$. Isolation cut is not applied in order to get the distribution in an extended region of isolation. Depending on the invariant mass region, the signal shape varies due to the radiation effect. This effect is estimated

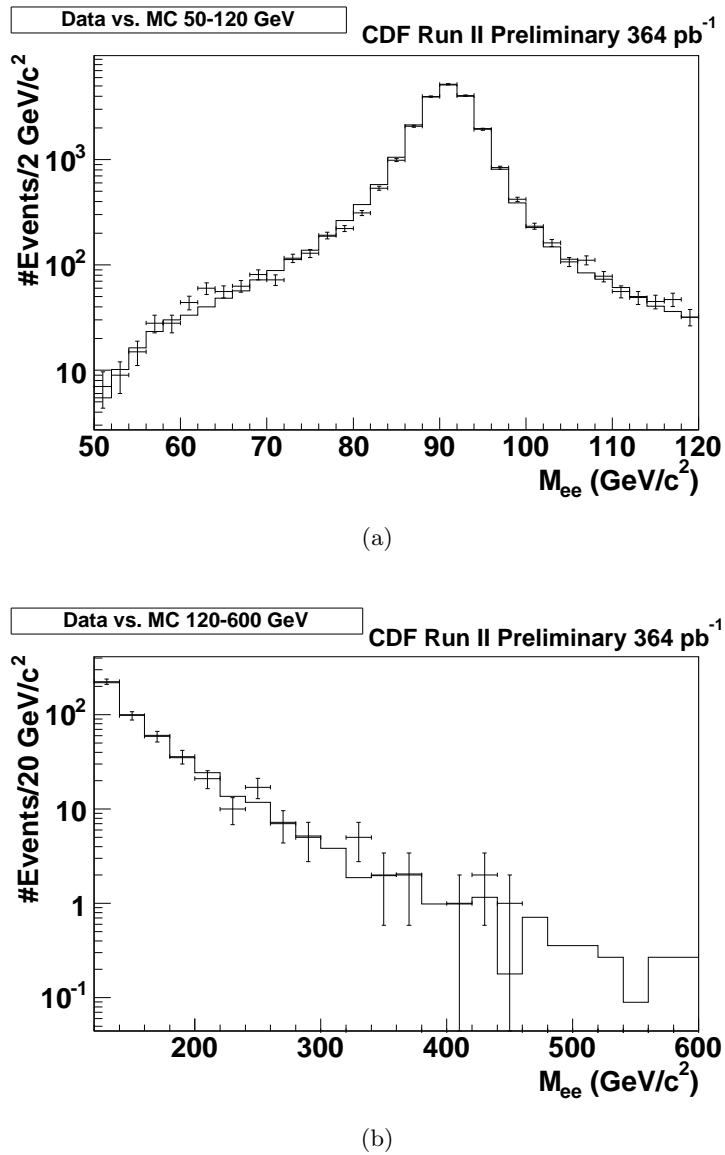


FIG. 1: The dielectron invariant mass distributions of data vs. Monte Carlo simulation. (a) Around the Z pole with 2 GeV bins. (b) Above the Z pole with 20 GeV bins.

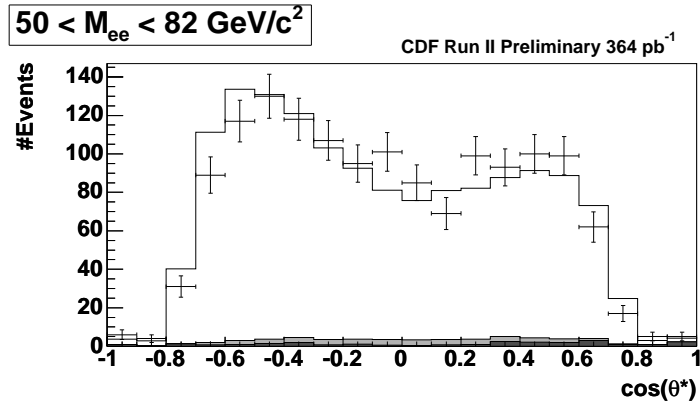
from the MC and applied to the template.

Jet template is obtained by removing W and Z events from the electron triggered events, and by requiring a back-to-back jet. We require the following criteria from the inclusive electron sample.

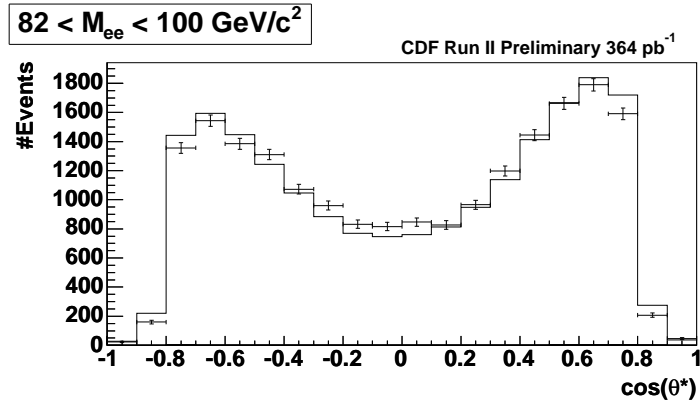
- No more than 1 EM object with EM $E_T > 10$ GeV.
- At least one jet objects with JET $E_T > 10$ GeV where $\Delta\phi$ between the EM object > 0.53 .

The electron selection cuts are applied to the electron-like object (except for the isolation cut), with a back-to-back jet in $r - \phi$ plane. Z events are removed by limiting the number of EM objects in the events to no more than one. Electrons from the W decay are removed from the knowledge of the missing transverse energy (MET).

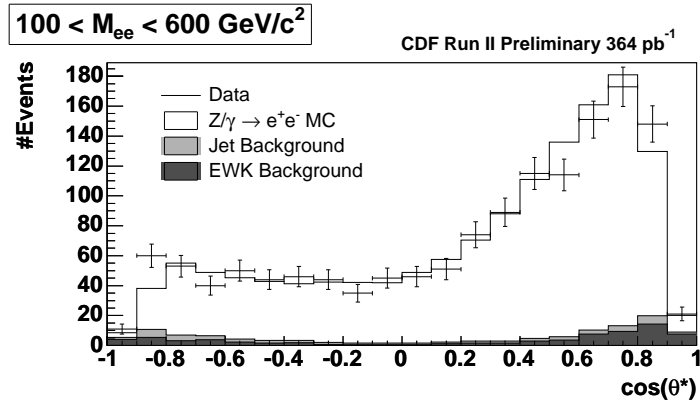
We use the fitter implemented in the ROOT library as a class TFractionFitter [2]. The fitter is capable of accounting for the uncertainties of the input templates. The fit is performed in two mass regions; below the Z pole and above the Z pole. The estimation is not sensitive around the Z pole region due to very small background rate. The background spectrum in the whole mass range is obtained from the dijet mass distribution, normalized to the fit result.



(a)



(b)



(c)

FIG. 2: The distribution of electron scattering angle $\cos \theta^*$. (a) Below the Z pole. (b) Around the Z pole. (c) Above the Z pole.

The dijet mass distribution is obtained by requiring the following conditions to the high p_T electron sample.

- No more than 1 EM object with EM $E_T > 10 \text{ GeV}$.
- At least one jet objects with JET $E_T > 10 \text{ GeV}$ with $\Delta\phi$ from the EM object > 0.53 .

- MET < 15 GeV.

Z is removed by requiring no more than 1 EM object. $W + jet$ events are rejected by the tight MET cut. The dijet mass shape is normalized to the constraints found from the isolation fits. The systematic uncertainty to the background estimation is estimated by varying the template shape, changing the cuts applied to get the signal shape and using the MC with extra material. The estimated number of background in CC and CP sample is summarized in the Table II.

B. Other Backgrounds

All other backgrounds from electroweak processes that include real electrons are estimated with MC. Such backgrounds include $t\bar{t}$ decaying into a final state with two electrons, $WW \rightarrow ll\nu\nu$, WZ with $Z \rightarrow e^+e^-$ and $W\gamma \rightarrow e\nu\gamma$. $W + jet$ background is an exception which is estimated by MC. The A_{FB} of the electroweak process backgrounds is accounted for the background subtraction.

Process	$\sigma \cdot \text{Br}$ (pb)	CC	CP	Total
Candidates	260	9455	13455	22910
Jet Background	-	12.8	130	142.8
$WW \rightarrow ll\nu\nu$	1.39	5.9	6.5	12.4
WZ ($Z \rightarrow e^+e^-$)	0.41	5.6	6.4	12.0
$W\gamma \rightarrow e\nu\gamma$	27.2	0.7	25.3	26.1
$W + \text{parton} \rightarrow e\nu + jet$	682.4	7.5	29.2	36.6
$t\bar{t}$ inclusive	5.50	3.2	1.9	5.1

TABLE II: Number of candidate events, Jet background estimated from the data, and EWK background estimated from Monte Carlo estimation.

IV. RESULT

Two million MC events are used to throw 11 pseudo experiments. Each pseudo experiments are unfolded by the inverted response matrix and the expected statistical uncertainty is calculated. The CDF Run II data with the integrated luminosity of 364 pb^{-1} is unfolded as Fig. 3. The χ^2/ndof with respect to the standard model is 10.9/12. The numbers of observed events and estimated backgrounds in each bins are listed in the Table III.

Bin	Mass (GeV)	Forward		Backward		Unfolded A_{FB}
		#Events	#BG	#Events	#BG	
1	50-65	13	9.6	16	7.6	-0.236
2	65-76	97	15.8	120	12.7	-0.389
3	76-82	207	9.5	284	7.3	-0.348
4	82-88	330	8.9	394	7.5	-0.102
5	88-94	1791	12.6	1817	10.1	0.044
6	94-100	6935	8.3	6295	6.8	0.471
7	100-106	1853	8.5	1348	6.0	0.303
8	106-120	333	18.6	169	13.3	0.432
9	120-140	288	14.9	130	11.9	0.555
10	140-200	166	22.7	58	14.7	0.512
11	200-300	140	7.5	53	4.1	0.571
12	300-600	45	0.8	15	0.7	0.668

TABLE III: Number of data and background, measured A_{FB} 's and their statistical errors.

The uncertainty of the energy scale is estimated from the Gaussian peak of the invariant mass as a function of the $|\eta_{det}|$ of the electron. Based on the distribution of the masses, the energy scale in the region of $|\eta| < 2.35$ is varied by 0.2 % and by 0.8 % where $|\eta| > 2.35$. The uncertainty of the energy resolution is found from the width of the Gaussian. We changed the resolution to increase the width by 0.3 GeV in the central region, by 0.2 GeV in the West

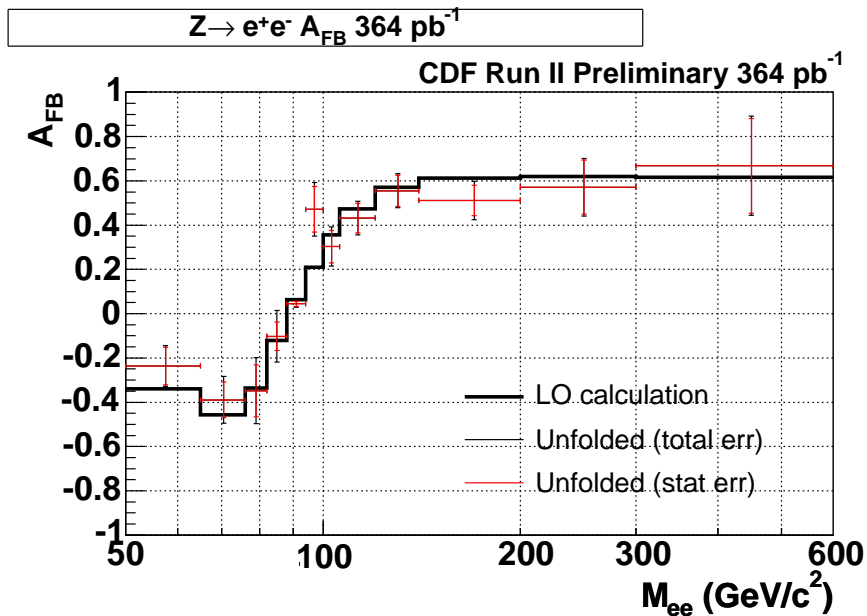


FIG. 3: The A_{FB} of the data of 364 pb^{-1} . The χ^2/ndof with respect to the leading order standard model is found to be 10.9/12.

plug, and by 0.4 GeV in the East plug region. These effects are applied to the 11 pseudo experiments and the shift in the measured A_{FB} was calculated. Two million MC events are simulated with two different material definitions. One is with 1% X_0 extra material in the central tracking region and the other is with 1/6 X_0 extra material in the plug region. The response matrices were applied to the 11 pseudo experiments to estimate the uncertainty. In order to estimate the uncertainty due to PDF, forty response matrices were made out of 40 error CTEQ6M PDF's. They are applied to the 11 standard pseudo experiments to determine the PDF uncertainty. We increased the background subtraction by 1σ and measured the effect on the A_{FB} . All the uncertainties are summarized in the Table IV.

Mass	Energy Scale	Energy Resol.	PDF	Material	Back-ground	Reponse Matrix	Total Syst.	Stat.	Total
50-65	0.009	0.020	0.003	0.015	0.018	0.018	0.037	0.085	0.092
65-76	0.010	0.006	0.002	0.060	0.016	0.027	0.069	0.081	0.106
76-82	0.017	0.047	0.001	0.041	0.008	0.067	0.093	0.117	0.149
82-88	0.030	0.063	0.003	0.062	0.002	0.023	0.096	0.064	0.116
88-94	0.022	0.005	0.001	0.008	0.000	0.002	0.010	0.011	0.015
94-100	0.028	0.033	0.002	0.037	0.001	0.030	0.064	0.103	0.121
100-106	0.018	0.014	0.001	0.033	0.005	0.029	0.050	0.073	0.088
106-120	0.011	0.007	0.000	0.026	0.012	0.017	0.036	0.067	0.076
120-140	0.005	0.015	0.000	0.018	0.018	0.015	0.034	0.070	0.077
140-200	0.004	0.009	0.000	0.041	0.030	0.017	0.054	0.069	0.087
200-300	0.006	0.016	0.001	0.022	0.030	0.030	0.051	0.122	0.130
300-600	0.000	0.034	0.001	0.049	0.012	0.042	0.074	0.214	0.224

TABLE IV: Summary of all the uncertainties. Statistical uncertainty is estimated from the 11 pseudo experiments. The material uncertainty is measured separately with the extra material in the central and plug, and then combined. The statistical uncertainty originating from the response matrix is included in the systematic uncertainty.

V. CONCLUSION

The forward backward charge asymmetry of the Z boson is unfolded with the CDF Run II data with integrated luminosity 364 pb^{-1} . The χ^2/ndof with respect to the standard model prediction is found to be 10.9/12.

-
- [1] M. Lefebvre *et. al.*, "Propagation of Errors for Matrix Inversion", hep-ex/990903.
[2] R. Barlow and C. Beeston, "Fitting using finite Monte Carlo samples", *Comp. Phys. Comm.* **77** 219 (1993).